Magnetic properties and crystal field in Pr_2 Zr_2 O_7

P. Bonville, S. Guitteny, A. Gukasov, I. Mirebeau, S. Petit, C. Decorse, M. Ciomaga Hatnean, G. Balakrishnan

Magnetic properties and crystal field in $Pr_2Zr_2O_7$

P. Bonville
SPEC, CEA, CNRS, Université Paris-Saclay, CEA-Saclay, 91191 Gif-sur-Yvette, France

S. Guitteny, A. Gukasov, I. Mirebeau,* and S. Petit
LLB, CEA, CNRS, Université Paris-Saclay, CEA-Saclay, 91191 Gif-sur-Yvette, France

C. Decorse
ICMMO/SP2M, Université Paris-Saclay, Université Paris-Sud, 91405 Orsay, France

M. Ciomaga Hatnean and G. Balakrishnan
Department of Physics, University of Warwick, Coventry CV4 7AL, United Kingdom
(Received 3 February 2016; revised manuscript received 2 September 2016; published 27 October 2016)

In this work, we revisit the crystal field acting on the non-Kramers Pr^{3+} ion ($4f^2$) in the quantum spin-ice candidate $Pr_2Zr_2O_7$ using both a standard calculation restricted to the ground spin-orbit multiplet and intermediate coupling states in the full basis of the f^2 configuration. Analysis of the thermal variation of the polycrystal magnetic susceptibility and of the local susceptibilities $\chi_\perp$ and $\chi_\parallel$ determined by means of polarized neutron diffraction experiments reveals that the effective antiferromagnetic exchange is strongly depleted at low temperature with respect to its high-temperature value. We then discuss the influence of crystal field imperfections arising from residual strains, which are especially important for a non-Kramers ion. We find that they are an essential ingredient to account for the very low temperature $M(H)$ magnetization curves, showing that the saturation is not achieved even at 8 T. Furthermore, as possible candidates to qualitatively understand the Curie-like behavior observed below 0.5 K, we discuss the influence of the magnetic hyperfine interaction.

DOI: 10.1103/PhysRevB.94.134428

I. INTRODUCTION

The pyrochlore lattice, made of tetrahedra connected through their summits and belonging to the cubic space group $Fd\bar{3}m$, has been the subject of intensive research for two decades because magnetic ions located on its vertices can be submitted to various types of geometrical frustration [1,2]. Materials with the general formula $R_2M_2O_7$, where R is a rare earth and M is a (nonmagnetic) metal, crystallize in the pyrochlore lattice. They exhibit a wealth of exotic magnetic properties, ranging from the so-called classical spin ice for ions with local Ising behavior like $Ho_2Ti_2O_7$ and $Dy_2Ti_2O_7$ [3,4] to candidates for "quantum" spin ices [5] like the still enigmatic $Tb_2Ti_2O_7$ [6,7]. In all these materials, either with Kramers (Dy^{3+}, Yb^{3+}) or non-Kramers (Ho^{3+}, Tb^{3+}) rare earths, the crystalline electric field (CEF) yields a magnetic doublet ground state well separated from the first excited state (several 100 K) except for $Tb_2Ti_2O_7$, where the excited doublet lies at 18 K above the ground state. For these materials, quantum spin-ice behavior should be characterized by an Ising-like ground state where fluctuations are, nevertheless, allowed between the two states of the doublet.

Recently, the pyrochlore material $Pr_2Zr_2O_7$, which contains the non-Kramers ion Pr^{3+}, was proposed as a possible quantum spin ice [5,8]. $Pr_2Zr_2O_7$ does not show magnetic ordering down to 0.076 K [9], although the small negative paramagnetic Curie temperature below 20 K [9,10] ($\theta_p \sim -0.5$ to -1 K) suggests weak antiferromagnetic interactions. The Pr^{3+} crystal electric field (CEF) level scheme was determined by inelastic neutron scattering (INS) in Ref. [8], yielding a doublet ground state separated by 120 K from the first excited state, a singlet. This level scheme is similar to that obtained in $Pr_2Ir_2O_7$ [11], $Pr_2Sn_2O_7$ [12], and $Pr_2Hf_2O_7$ [13], where no magnetic ordering has been detected either and which are also possible quantum spin ices.

In this work, we obtain a new CEF level scheme in $Pr_2Zr_2O_7$ first by restricting the study to the ground spin-orbit multiplet and then by using the complete basis of $4f^2$ states [14]. We then investigate the local susceptibilities $\chi_\perp$ and $\chi_\parallel$ determined by means of polarized neutron diffraction experiments. Their thermal variation suggests that the strength of the antiferromagnetic effective exchange interaction strongly decreases between high ($\sim$300 K) and low ($T < 20$ K) temperature. We finally compute the $M(H)$ profiles and compare them to recent available single-crystal magnetic measurements [15]. To account qualitatively for the experiments, especially the absence of quick saturation of the magnetization at very low temperature, the influence of crystal-field imperfections breaking the local trigonal symmetry is discussed. Such terms typically arise from residual strains coupled to the electronic density and play an important role for non-Kramers ions. The Curie-like behavior observed below 0.5 K, with an upturn of the susceptibility, both in $Pr_2Zr_2O_7$ and in $Pr_2Hf_2O_7$ [13] remains an issue. The magnetic hyperfine interaction is shown to induce such a Curie-like behavior at low temperature, but its magnitude is too small to account for the data.

A preliminary account of this work was presented in Ref. [16].

II. EXPERIMENT

The polycrystalline sample was prepared by solid-state reaction. Stoichiometric quantities of at least 99.9% purity

*isabelle.mirebeau@cea.fr

Pr_6O_{11} and ZrO_2 starting powders were mixed thoroughly and ground together, then compressed into pellets. The mixture was heated up to 1500°C in air for several days with intermediate grindings. The final powder was annealed in a H_2(10%)-Ar flow at 1200°C for 2 d. The single crystal was grown using the floating-zone technique as described in Ref. [17]. The same thermal treatment as for the powder, under reducing atmosphere, was then applied. The obtained products showed a green color.

The local susceptibility was measured on the single-crystal sample by in-field polarized neutron diffraction (PND) [18]. The neutron measurements were performed at the ORPHÉE reactor of the Laboratoire Léon Brillouin. Polarized neutron flipping ratios were measured on the Super-6T2 spectrometer [19] using incident neutrons of wavelength $\lambda = 1.4$ Å and polarization $P_0 = 0.98$. Flipping ratios were measured in the temperature range from 2 to 270 K in magnetic fields of 1 and 6 T applied parallel to the [110] direction. The CHILSQ program developed for the analysis of PND data for anisotropic paramagnetic compounds was used to refine the flipping-ratio data by the least-squares method [20].

III. ANALYSIS OF THE CRYSTAL FIELD IN THE COMPLETE BASIS OF f^2 STATES

The point-group symmetry at each of the four rare-earth sites in the pyrochlore unit cell is D_{3d}, with the threefold axes being parallel to ⟨111⟩-type directions. Choosing this axis as the z axis, the CEF Hamiltonian is written as

$$\mathcal{H}_{CEF} = B_0^2 C_0^2 + B_0^4 C_0^4 + B_3^4 C_3^4 + B_0^6 C_0^6 + B_3^6 C_3^6 + B_6^6 C_6^6, \quad (1)$$

where B_n^m are parameters and C_n^m are tensorial operators [21].

In Ref. [8], the inelastic neutron data were interpreted in the frame of the Stevens-operator method (ground multiplet $^3H_4$), and the following CEF level scheme was determined: a ground doublet, a singlet at 10 meV, a doublet at 57 meV, then two singlets (82 and 93 meV) and a doublet (109 meV). The corresponding B_n^m parameters are shown in Table I. The calculated inelastic spectrum, obtained with a single linewidth $\Gamma = 0.5$ meV for all lines, is shown in Fig. 1 (black line), together with the estimated experimental line intensities from Ref. [8], scaled to that of the 10 meV line.

The questionable agreement with experiment, the too large calculated magnetic moment $3.0\mu_B$ (instead of $2.5\mu_B$ experimentally), and the strong differences with the B_n^m coefficients reported for the related Pr^{3+}-based compound $Pr_2Sn_2O_7$ [12] call for a new study. Using the experimental magnetic moment, the energy levels, and relative intensities as constraints, we have obtained a new set of fitted parameters, more consistent with the latter study and reproducing well the above level scheme (see Table I) except for one unimportant difference: the two highest levels are a doublet (93 meV) and a singlet (109 meV). The calculated inelastic spectrum is shown in Fig. 1 (green line). The line intensities of the two lower-energy lines are seen to be equivalent in the two sets and not far from the experimental value. As to the three high-energy lines, the comparison is clearly in favor of the new set, especially for the 110 meV line, whose intensity was overestimated. Finally, the calculated effective magnetic moment μ_{eff} is better reproduced with a calculated value of $2.7\mu_B$.

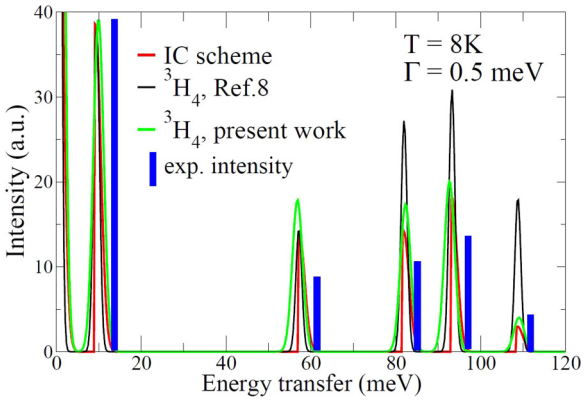

FIG. 1. Inelastic neutron spectrum for $Pr_2Zr_2O_7$ calculated at 8 K using the IC scheme (red line, parameters in Table II) and restricted to the $^3H_4$ multiplet (black line, parameters in Table I). The blue bars are approximate values for the experimental intensities from Ref. [8].

As pointed out in Ref. [12], the ground spin-orbit multiplet of Pr^{3+} ($4f^2$) is $^3H_4$ ($J = 4$, $g_J = 4/5$) separated by about 2000 K from the first excited multiplet $^3H_5$. The crystal electric field splits each multiplet by about 1000 K, and therefore, it is to be expected that higher-energy multiplets can slightly admix within the ground $^3H_4$ state. To take this into account, we diagonalized the crystal-field Hamiltonian using the 91 intermediate-coupling (IC) basis states of Pr^{3+} (program SPECTRE [14]) instead of the Stevens-operator-equivalent method [22,23] limited to the ground spin-orbit multiplet (nine states). For our calculation using the IC scheme, we used these B_n^m values as starting parameters and these energies as constraints for the fit with the program SPECTRE. We obtained a set of fitted parameters reproducing well the above level scheme (see Table II) with again a doublet (93 meV) and a singlet (109 meV) for the highest-energy levels. The calculated intensities (red line in Fig. 1) reproduce fairly well the experiment, while the calculated effective magnetic moment $2.5\mu_B$ corresponds exactly to the measured value.

TABLE I. CEF parameters B_n^m (in μeV) determined in the ground multiplet $^3H_4$ for $Pr_2Sn_2O_7$ [12] and $Pr_2Zr_2O_7$ (present work and from Ref. [8]).

	B_0^2	B_0^4	B_3^4	B_0^6	B_3^6	B_6^6
$Pr_2Zr_2O_7$						
Ref. [8]	−928	−36.2	295	0.664	−2.28	4.35
This work	−631	−32.36	−467.4	0.245	1.464	−1.907
$Pr_2Sn_2O_7$ [12]	−733	−36.5	−383	0.278	0.0328	−4.59

TABLE II. CEF parameters B_n^m (in μeV) for $Pr_2Zr_2O_7$ from the present work (IC scheme).

B_0^2	B_0^4	B_3^4	B_0^6	B_3^6	B_6^6
−504.8	−33.6	−486.9	0.473	−3.60	−3.25

The ground-state doublet in this IC scheme, including the largest mixing terms from the excited spin-orbit multiplets $^1G_4$ and $^3H_5$, is

$$|\psi_g\rangle = 0.800|^3H_4, \pm 4\rangle - 0.496|^3H_4, \pm 1\rangle - 0.144|^3H_4, \mp 1\rangle - 0.232|^3H_4, \mp 4\rangle + 0.138|^1G_4, \pm 4\rangle - 0.087|^1G_4, \pm 1\rangle - 0.040|^1G_4, \mp 4\rangle - 0.048|^3H_5, \pm 4\rangle + \cdots . \quad (2)$$

Therefore, although the excited spin-orbit multiplets lie at 200 meV and more above the ground state, quantum mixing into the ground state is not negligible. We note, however, that $|\psi_g\rangle$ is close to the ground wave function determined to restrict the calculation to $^3H_4$,

$$|\psi'_g\rangle = 0.894|^3H_4, \pm 4\rangle \pm 0.447|^3H_4, \pm 1\rangle - 0.024|^3H_4, \mp 2\rangle, \quad (3)$$

but rather different from the ground state obtained in Ref. [8]:

$$|\psi''_g\rangle = 0.963|^3H_4, \pm 4\rangle \pm 0.252|^3H_4, \pm 1\rangle - 0.094|^3H_4, \mp 2\rangle. \quad (4)$$

It is worth noting that when computing the magnetic moment induced by a magnetic field, one important difference between the Stevens-operator method and the IC scheme calculation lies in the transverse magnetization, i.e., the magnetization induced by a field perpendicular to the local ternary axis. The transverse magnetization in the two cases at 1.7 K for the crystal-field parameters of Table I for the $^3H_4$ calculation and of Table II for the IC scheme is represented in Fig. 2. It is much larger in the IC scheme calculation, which means that the admixture of excited states in the ground state by the field is more important. The transverse magnetization is needed to compute the single-crystal magnetization in pyrochlores due to the presence of four sites with different symmetry-axis directions. Therefore, even when the field is along one of the threefold axes, the other sites experience a transverse component of the magnetic field.

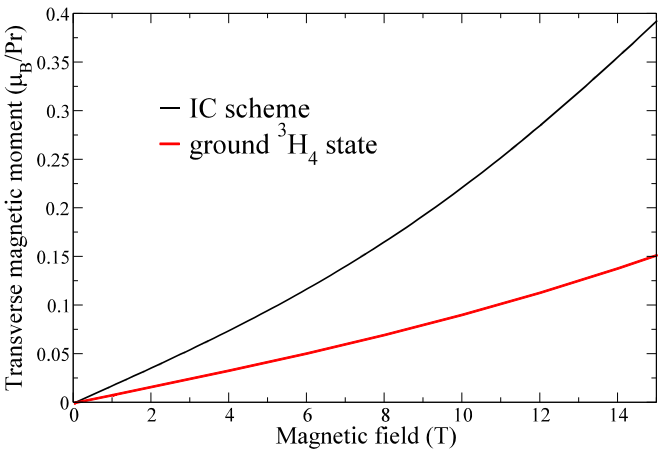

FIG. 2. Magnetization at 1.7 K induced by a magnetic field perpendicular to a ternary ⟨111⟩-type axis in the two types of CEF calculations.

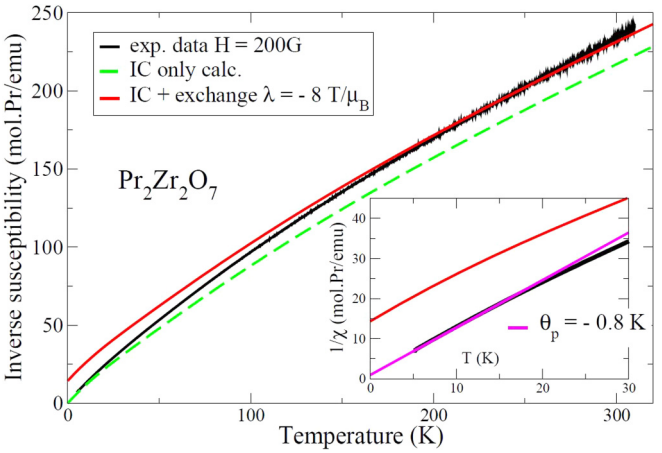

FIG. 3. Thermal variation of the polycrystal inverse magnetic susceptibility measured with $H = 200$ G (black line). The green dashed line represents the calculation using the IC scheme CEF parameters in Table II, and the red line shows the exchange-corrected CEF calculation. The inset shows the low-temperature range; the magenta line is a Curie-Weiss law with $\theta_p = -0.8$ K.

IV. COMPARISON WITH MAGNETIC MEASUREMENTS

A. The bulk susceptibility

The inverse powder magnetic susceptibility $1/\chi(T)$ is shown in Fig. 3. The calculated $1/\chi_0(T)$ arising from the crystal field in the IC scheme is represented by the green dashed line. At high temperature, the data are parallel to $1/\chi_0(T)$ and lie above it. They can be reproduced by introducing Antiferromagnetic (AF) exchange as a perturbation via an isotropic (negative) molecular field constant λ:

$$1/\chi(T) = 1/\chi_0(T) - \lambda. \quad (5)$$

This is the red solid curve in Fig. 3, with $\lambda = -8.0(1)\,\mathrm{T}/\mu_B = -14.3$ mol Pr/emu, in very good agreement with the value −14.6 mol Pr/emu obtained in Ref. [8]. The high-temperature effective moment is $\mu_{\mathrm{eff}} \simeq 3.55\mu_B$, close to the free-ion value for the Pr^{3+} ion ($3.57\mu_B$). So, at high temperature, the IC scheme and the Stevens-operator method yield the same result for $\chi_0(T)$.

As temperature decreases below 150 K, the data deviate from the red curve and almost join the crystal-field-only calculation below 30 K. The inset of Fig. 3 shows that $1/\chi(T)$ obeys a Curie-Weiss law below 20 K with $\mu_{\mathrm{eff}} = 2.55\mu_B$ and $\theta_p \simeq -0.8$ K (magenta line). This effective moment value is the same as that measured previously in the very low temperature range with **H** // [111] (see Refs. [8,10]).

But it is clear from the inset of Fig. 3 that the molecular field constant has strongly decreased (in absolute value) from its high-temperature value. It can be estimated using the following mean-field expression:

$$k_B\theta_p^{bT} = \tfrac{1}{3}\lambda_{bT}\,\mu_{\mathrm{eff}}^2. \quad (6)$$

Using $\theta_p^{bT} \simeq -1$ K, we obtain $\lambda_{bT} \simeq -0.54\ \mathrm{T}/\mu_B$, about 15 times smaller than the high-temperature value of $-8\ \mathrm{T}/\mu_B$. Therefore, we must conclude that the effective exchange has decreased on cooling, while remaining of AF type. This could be caused by a modification of the exchange path as

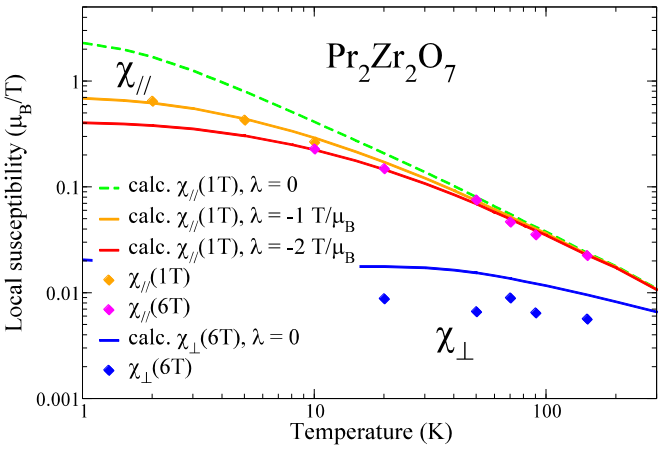

FIG. 4. Thermal variation of the local susceptibility measured by neutron diffraction with fields of 1 and 6 T. The lines are calculations using the full IC scheme with the bare CEF ($\lambda = 0$) and adding exchange in perturbation ($\lambda \neq 0$).

temperature decreases, for instance, a reduction of a Pr-O-Pr bridge angle. It could also be accounted for by a competition between AF and ferromagnetic interactions, the latter starting to develop as temperature decreases and almost canceling the former below about 20 K. The onset of ferromagnetic correlations at low temperature, while the high-temperature exchange is AF, has previously been observed in $Tb_2Sn_2O_7$ [24].

B. The single-crystal local susceptibility

As reported for other rare-earth pyrochlore magnets [25–27], the local susceptibility tensor $\tilde{\chi}$ can be determined by in-field polarized neutron diffraction by measuring the flipping ratios [25]. We show in Fig. 4 the components of the susceptibility parallel ($\chi_\parallel$) and perpendicular ($\chi_\perp$) to the local $\langle 111 \rangle$ directions obtained by refining the flipping ratios taken at 1 and 6 T at different temperatures. The Ising character of the Pr^{3+} ion for these field values is clear, with $\chi_\parallel/\chi_\perp \simeq 30$ at low temperature.

The bare CEF susceptibility tensor was calculated using the full IC scheme. The $\chi_\perp(T)$ curve (blue line in Fig. 4) shows an order of magnitude agreement with the data, whereas the $\chi_\parallel(T)$ curve (green line in Fig. 4) lies somehow above the data. Introducing isotropic exchange via expression (5), an antiferromagnetic (negative) value $\lambda = -1.5(5)$ T/μ_B leads to good agreement with the data (orange and red curves). This value is intermediate between the high-temperature (-8 T/μ_B) and the low-temperature (-0.54 T/μ_B) values determined in the previous paragraph, and it must be considered an average value. As to the calculation within the $^3H_4$ multiplet (not shown), it yields a somewhat worse agreement with experiment, especially at low temperature.

C. Low-temperature magnetization

In this section, we calculate the single-crystal $M(H)$ curves at 0.1 K for three orientations of the magnetic field ([100], [111]. and [110]) using the IC scheme and compare them to recent experimental data [15] reproduced in Fig. 5. Unexpectedly for an Ising magnet, the magnetization is not fully saturated, even at 8 T. The reached magnetization is different along the three directions, as predicted for such Ising spins with a multiaxis anisotropy [3]. Nevertheless, the ratio between the obtained values is smaller than the expected ratio ($M_{[100]}/M_{[111]} = \sqrt{3}/2$, $M_{[110]}/M_{[111]} = \sqrt{6}/2$), suggesting that the apparent anisotropy is reduced compared to the case of a classical Ising spin. As shown in the inset of Fig. 5, a departure from the Curie-Weiss law occurs below 0.5 K as a

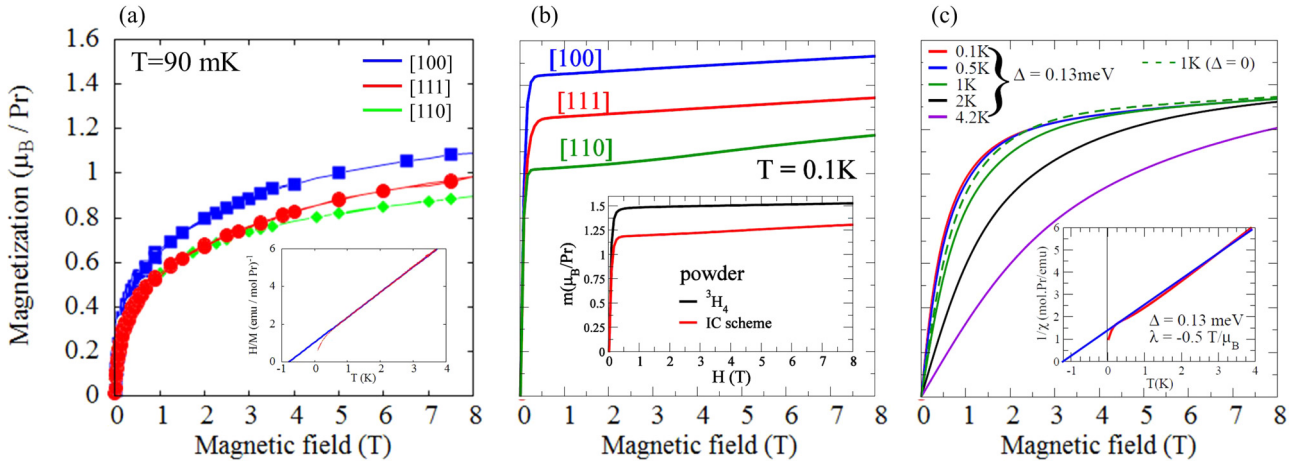

FIG. 5. (a) M vs H at 90 mK reproduced from Ref. [15] for the field applied along the [111] (red circles), [110] (green diamonds), and [100] (blue squares) directions of the sample. Inset: H/M vs T in $\mu_0 H = 9$ mT. The thick blue line is a fit to the Curie-Weiss law between 1 and 4.2 K: $H/M = 1.055 + 1.328T$. (b) Calculated single-crystal magnetization curves at $T = 0.1$ K for a magnetic field along [100], [111], and [110], using the IC scheme with parameters as shown in Table II. Inset: powder magnetizations at $T = 0.1$ K using both types of calculation schemes. (c) Isothermal magnetization curves calculated with the IC scheme between 0.09 and 4.2 K for **H** // [111] and a ground-state splitting $\Delta = 0.13$ meV (solid lines) and at 1 K for $\Delta = 0$ (dashed curve). Inset: calculated susceptibility in the same temperature range with $\Delta = 0.13$ meV and in the presence of the hyperfine interaction (red curve). The blue curve is a Curie-Weiss law with $\mu_{\text{eff}} \simeq 2.5\mu_B$ and $\theta_p \simeq -1.2$ K.

Curie-like increase of the susceptibility. A similar effect was also reported in $Pr_2Hf_2O_7$ [13] in the same temperature range.

Confrontation to calculated M(H) using CEF schemes

Calculations using the IC scheme are shown in Fig. 5(b). Due to the degenerate magnetic ground state, (quasi)saturation occurs at 0.5 T at such a low temperature. The Ising character of the ground doublet implies that the high-field magnetization values follow the well-known sequence in pyrochlore systems: the largest occurs for **H** // [100], then for **H** // [111] and for **H** // [110]. Self-consistent exchange was not introduced since the program SPECTRE does not allow it (the perturbation approach is also not valid for the magnetization). We also computed the powder magnetization $M_{\rm poly}$ according to the following average:

$$M_{\rm poly}(H) = \tfrac{1}{13}[3M_{[001]} + 4M_{[111]} + 6M_{[110]}]. \qquad (7)$$

It is close to the [111] magnetization, which is a general property in pyrochlores. The following then emerges from the comparison between these data and the calculated curves (Fig. 5).

Magnetic moment at saturation. Looking first at the powder magnetization in the two types of calculations [inset of Fig. 5(b)], it is clear that the (quasi)saturation moment value is higher by about $0.25\mu_B$ in the $^3H_4$ calculation. This is due to the fact that the powder saturation value is close to $1/2\ \mu_{\rm eff}$ for an Ising system. As determined in Sec. III, the IC scheme $\mu_{\rm eff}$ value is $2.5\mu_B$, and the Stevens-operator method value is $3\mu_B$ [8], resulting in the observed difference. The single-crystal magnetization curves are also shifted down by about $0.25\mu_B$ when using the IC scheme.

The IC scheme leads, however, to calculated curves still too high by about $0.3\mu_B$: at 8 T, $1.33\mu_B$ vs $1.0\mu_B$ for the calculated and experimental [111] values, respectively. The presence of antiferromagnetic exchange, detected in the susceptibility data described in Sec. IV B, would deplete the calculated values but not to such a large extent.

Slope of M(H) at large fields. Another difference lies in the slope of the linear (quasi)saturation: it is more pronounced for the IC scheme curves than for the $^3H_4$ curves. This is due to the enhanced induced transverse magnetization in the IC scheme.

Low-field behavior. The calculated curves saturate very rapidly, above about 0.5 T, while the data show no saturation but a smooth curvature. This discrepancy cannot be solved by introducing an exchange interaction. In the paramagnetic range, introducing AF exchange of the order of 1 K will only slightly reduce the saturation value without changing the shape of the curve. At 0.1 K, it will yield an ordered antiferromagnetic state and therefore a weak linear $M(H)$ variation, in contradiction with experiment.

V. DISCUSSION

The calculated rapid saturation of $M(H)$ is characteristic of a degenerate (Ising) magnetic doublet, which is indeed the nominal CEF ground state in $Pr_2Zr_2O_7$. The important curvature of the data points thus to a degeneracy lifting, which could be due to some extra interaction locally breaking the threefold symmetry. Non-Kramers doublets are known to be sensitive to crystal-field imperfections, to quadrupole-quadrupole interactions, etc., which lift the degeneracy of the CEF doublets and yield two singlet states as ground states. The degeneracy lifting should be in the range 0.1–1 K, which means that its effect should be stronger at the base temperature (0.1 K) and progressively disappear as temperature increases.

In this picture, the CEF ground state is a singlet, so the susceptibility is expected to be constant at low temperature, in contradiction with experiment. We thus must invoke another interaction restoring a Curie-like law at very low temperature. A possible candidate is the hyperfine interaction of the $I = 5/2$ nuclear spin of ^{141}Pr with the electronic degrees of freedom. It will change this singlet ground state into a set of degenerate doublets and then to a Curie-like behavior.

Actually, these two interactions are naturally expected to play a significant role at very low temperature and should be present in a description of the properties of a non-Kramers ion. In the following, we examine these hypotheses and compute the magnetization curves for **H** // [111].

A. Local imperfections of the crystal field

In order to model local imperfections of the crystal field, we introduced a nontrigonal component of the crystal field (1) of the type $B_2^2C_2^2$. Here, B_2^2 represents the magnitude of a strain coupled to one quadrupole operator (C_2^2). It would be more realistic to take into account a distribution of B_2^2, leading to a distribution of splittings; this more complex hypothesis will be examined in a future publication. We note also that such a term would naturally appear, at the mean-field level, in the context of quadrupole-quadrupole interactions. In that case, B_2^2 would model the quadrupolar mean field experienced by a given ion [15,28].

We find that such a term induces a splitting of the ground doublet, with magnitude $\Delta \sim 4.66 \times B_2^2$. We then proceeded to the simulation of the magnetization curves at various temperatures between 0.1 and 4.2 K. We find that a value $B_2^2 = -27\ \mu$eV, inducing a splitting $\Delta \simeq 0.13$ meV, yields a qualitative overall agreement with the data in the temperature range 0.1–4.2 K [see Fig. 5(c)]. The presence of the nontrigonal component suppresses the fast saturation below about 1 K ($\sim\Delta$) because the ground state is a singlet and the magnetization at low field is due to quantum mixing with the upper state at an energy Δ, in qualitative agreement with experiment.

B. Hyperfine interaction

As to the magnetic hyperfine interaction with the spin $I = 5/2$ of the ^{141}Pr nucleus, we will treat it for the sake of simplicity in the ground spin-orbit multiplet, where it is written as

$$\mathcal{H}_{hf} = A\mathbf{I}\cdot\mathbf{J}, \qquad (8)$$

where $A = 0.055$ K and the quadrupolar hyperfine interaction is negligible [29]. When projected onto the degenerate Ising ground doublet, it reduces to the diagonal form $\mathcal{H}_{hf} = AI_zJ_z$. The eigenstates are $|\psi_g\rangle|m\rangle$, where m is the nuclear quantum number varying between $-5/2$ and $5/2$. The electronuclear eigenstates have Ising character, and it can be shown that the susceptibility is unchanged with respect to the pure electronic

value. The situation is different when the ground doublet is split by an energy Δ due to crystal-field imperfections or quadrupolar interactions. As shown in the Appendix, in the case $\Delta \gg A$, the eigenstates of the electronuclear system are six degenerate doublets with energies

$$E_{\pm,m} \simeq \Delta \pm \frac{\zeta^2 A^2 m^2}{\Delta} \tag{9}$$

and magnetic moment

$$\mu_{\pm,m} \simeq \mp g_J \mu_B \frac{2\zeta^2 A m}{\Delta}, \tag{10}$$

with $\zeta = \langle \psi_g | J_z | \psi_g \rangle$. Since the two states of each doublet have opposite magnetic moments, their susceptibility is Curie-like, and so is the susceptibility of the electronuclear system, calculated in the Appendix in the Stevens-operator-equivalent scheme. The inset of Fig. 5(c) represents the inverse susceptibility of the electronuclear system obtained with the same splitting value as used for the magnetization calculation, $\Delta = 0.13$ meV, and with a matrix element of J_z such that $\zeta = \mu_{\rm eff}/(g_J \mu_B) = 3.12$. We also introduced a molecular field constant $\lambda = -0.5\ {\rm T}/\mu_B$ to account for the negative θ_p value, as explained above. A deviation from the Curie-Weiss law due to the hyperfine coupling indeed occurs below about 0.5 K, yielding a downturn as experimentally observed [see inset of Fig. 5(a)], but the agreement is still not fully satisfactory.

VI. CONCLUSION

The present study yields the following main results, which should be taken into account for an improved description of the $Pr_2Zr_2O_7$ ground state and of its low-energy excitations:

(i) Our study of the crystal field in terms of schemes restricted either to the ground multiplet or to intermediate states in the whole basis for the Pr^{3+} ion yields a fairly reasonable description of the neutron inelastic data, as well as of the temperature evolution of the bulk and local susceptibilities.

(ii) The strong Ising character is attested by local susceptibility measurements; we could estimate it by the ratio $\chi_{//}/\chi_{\perp} \sim 30$ near $T = 0$ in a 1-T field. The effective exchange interaction is found to be antiferromagnetic, but the data suggest a strong depletion at low temperature in the 10 K range. Defining an ionic nearest-neighbor effective exchange integral by $z J_{\rm eff} = k_B \theta_p$, where $z = 6$ is the number of first neighbors, one obtains at low temperature $J_{\rm eff} \simeq -0.13$ K, whereas it reaches -3.8 K near room temperature.

(iii) We suggest that strains coupled to the electronic density, interactions between quadrupolar moments, and the hyperfine interaction should be taken into account in the microscopic Hamiltonian describing $Pr_2Zr_2O_7$. A degeneracy lifting of the ground non-Kramers doublet by crystal-field imperfections or quadrupole-quadrupole interactions is an appealing candidate to understand the low-temperature behavior and especially the absence of saturation in $M(H)$ curves even at 8 T. The order of magnitude of the degeneracy lifting is about 1 K, and it is worth noting that the low-temperature $J_{\rm eff}$ is of the same order of magnitude. Although this leads to a breakdown of the Ising property of the ground doublet, a strong Ising anisotropy is recovered in a moderate magnetic field.

The magnetic hyperfine interaction with the spin of the ^{141}Pr nucleus leads to a Curie-like increase of the susceptibility below 0.5 K, yet the comparison with experiment is not fully satisfactory.

Moreover, since any odd operator like the moment $\boldsymbol{\mu} = -(\mathbf{L} + 2\mathbf{S})\mu_B$ has no matrix elements between the two states of a degenerate non-Kramers doublet, the low-energy magnetic fluctuations observed experimentally [8] cannot arise from bilinear exchange since the corresponding matrix elements are zero. This means that quadrupolar degrees of freedom are a natural candidate for the main source of (quantum) dynamics in $Pr_2Zr_2O_7$. We note that similar effects have been invoked in the non-Kramers compound $Tb_2Ti_2O_7$ [7,30,31]. As noticed in Ref. [12] for $Pr_2Sn_2O_7$, the IC description of the crystal field markedly increases the expectation value of the quadrupole operators (by a factor of $\sim$3) with respect to the Stevens-operator-equivalent method. The use of IC basis states should thus provide a better starting point for the description of those degrees of freedom.

ACKNOWLEDGMENTS

We thank A. T. Boothroyd for making available to us the program SPECTRE and E. Lhotel for the low-temperature magnetization data reproduced from Ref. [15]. M.C.H. and G.B. acknowledge financial support from EPSRC, United Kingdom, Grant No. EP/M028771/1.

APPENDIX: THE ELECTRONUCLEAR SYSTEM IN THE GROUND DOUBLET IN THE PRESENCE OF SPLITTING AND HYPERFINE INTERACTION

In this appendix, we will use the Stevens-operator-equivalent scheme, where J is a good quantum number, for simplicity to compute the susceptibility of the electronuclear system $^{141}Pr^{3+}$, with nuclear spin $I = 5/2$. We consider only the degenerate ground doublet $\{|\psi_g\rangle, |\bar{\psi}_g\rangle\}$ (2), assumed to be submitted to a nontrigonal crystal-field term like $B_2^2 C_2^2$, where $C_2^2 = \frac{1}{2}(J_+^2 + J_-^2)$. Setting $\Delta = B_2^2 \langle \bar{\psi}_g | C_2^2 | \psi_g \rangle$, the matrix of the crystal field restricted to the doublet is

$$\mathcal{H}_{CEF} = \begin{pmatrix} 0 & \Delta \\ \Delta & 0 \end{pmatrix}. \tag{A1}$$

The new eigenstates are the entangled symmetric and antisymmetric states (dropping the bras and kets):

$$\psi_s = \frac{1}{\sqrt{2}}(\psi_g + \bar{\psi}_g), \quad \psi_a = \frac{1}{\sqrt{2}}(\psi_g - \bar{\psi}_g), \tag{A2}$$

which we will dub the "tunnel" states, in analogy with the tunneling effect. These states are singlets separated by an energy Δ, and they bear no intrinsic magnetic moment. The following property holds for these states:

$$\langle \psi_s | J_z | \psi_a \rangle = \langle \psi_g | J_z | \psi_g \rangle = \zeta. \tag{A3}$$

We now consider the effect of a Zeeman term $\mathcal{H}_Z = g_J \mu_B H J_z$, with the field $\mathbf{H}$ applied along the ternary axis Oz, and of the magnetic hyperfine interaction $\mathcal{H}_{hf} = A I_z J_z$ in the basis $\{\psi_s; m, \psi_a; m'\}$. The total corresponding 12×12

Hamiltonian

$$\mathcal{H} = \mathcal{H}_{CEF} + \mathcal{H}_Z + \mathcal{H}_{hf} \tag{A4}$$

is diagonal in the nuclear states and decomposes into six 2×2 blocks for each m value. The matrix of one block, using the notation $h = g_J \mu_B H$, is written

$$B_m = \begin{pmatrix} 0 & (mA+h)\zeta \\ (mA+h)\zeta & \Delta \end{pmatrix}. \tag{A5}$$

After diagonalization of the six blocks and setting $D(m,h) = \sqrt{\Delta^2 + [2\zeta(mA+h)]^2}$, one obtains the magnetization:

$$M = 2 g_J \mu_B \zeta^2 \frac{\sum_m \frac{mA+h}{D(m,h)} \sinh \frac{D(m,h)}{2T}}{\sum_m \cosh \frac{D(m,h)}{2T}}. \tag{A6}$$

From this expression, the powder magnetization or the magnetization along [111] in the pyrochlore lattice is easily obtained. The powder susceptibility for chosen values of the splitting Δ is represented in Fig. 6. The departure from the Curie-Weiss law (black curve) is clearly visible, as well as the Curie-like increase at lower temperature.

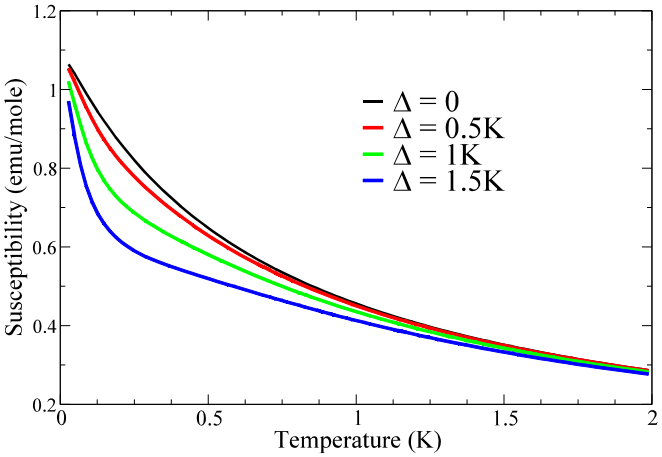

FIG. 6. Low-temperature powder magnetic susceptibility for a field $H = 200$ G in the presence of magnetic hyperfine coupling for different values of the ground-state splitting Δ.

[1] J. S. Gardner, M. J. P. Gingras, and J. E. Greedan, Rev. Mod. Phys. **82**, 53 (2010).

[2] *Introduction to Frustrated Magnetism*, edited by C. Lacroix, P. Mendels, and F. Mila (Springer, Berlin, 2011).

[3] M. J. Harris, S. T. Bramwell, P. C. W. Holdsworth, and J. D. M. Champion, Phys. Rev. Lett. **81**, 4496 (1998).

[4] A. P. Ramirez, A. Hayashi, R. J. Cava, R. Siddhartan, and B. S. Shastry, Nature (London) **399**, 333 (1999).

[5] M. J. P. Gingras and P. A. McClarty, Rep. Prog. Phys. **77**, 056501 (2014).

[6] H. R. Molavian, M. J. P. Gingras, and B. Canals, Phys. Rev. Lett. **98**, 157204 (2007).

[7] P. Bonville, A. Gukasov, I. Mirebeau, and S. Petit, Phys. Rev. B **89**, 085115 (2014).

[8] K. Kimura, S. Nakatsuji, J. J. Wen, C. Broholm, M. B. Stone, E. Nishibori, and H. Sawa, Nat. Commun. **4**, 1934 (2013).

[9] K. Matsuhira, C. Sekine, C. Paulsen, M. Wakeshima, Y. Hinatsu, T. Kitazawa, Y. Kiuchi, Z. Hiroi, and S. Takagi, J. Phys. Conf. Series **145**, 012031 (2009).

[10] K. Kimura, S. Nakatsuji, and A. A. Nugroho, J. Korean Phys. Soc. **63**, 719 (2013).

[11] Y. Machida, S. Nakatsuji, H. Tonomura, T. Tayama, T. Sakakibara, J. van Duijn, C. Broholm, and Y. Maeno, J. Phys. Chem. Solids **66**, 1435 (2005).

[12] A. J. Princep, D. Prabhakaran, A. T. Boothroyd, and D. T. Adroja, Phys. Rev. B **88**, 104421 (2013).

[13] R. Sibille, E. Lhotel, M. Ciomaga Hatnean, G. Balakrishnan, B. Fåk, N. Gauthier, T. Fennell, and M. Kenzelmann, Phys. Rev. B **94**, 024436 (2016).

[14] A. T. Boothroyd, SPECTRE, a program for calculating spectroscopic properties of rare earth ions in crystals (1990–2015).

[15] S. Petit, E. Lhotel, S. Guitteny, O. Florea, J. Robert, P. Bonville, I. Mirebeau, J. Ollivier, H. Mutka, E. Ressouche, C. Decorse, M. Ciomaga Hatnean, and G. Balakrishnan, Phys. Rev. B **94**, 165153 (2016).

[16] S. Guitteny, Ph.D. thesis, Paris-Sud University, 2015.

[17] M. Ciomaga Hatnean, C. Decorse, M. R. Lees, O. A. Petrenko, D. S. Keeble, and G. Balakrishnan, Mater. Res. Express **1**, 026109 (2014).

[18] A. Gukasov and P. J. Brown, J. Phys. Condens. Matter **14**, 8831 (2002).

[19] A. Gukasov, A. Goujon, J.-L. Meuriot, Ch. Person, G. Exil, and G. Koskas, Phys. B (Amsterdam, Neth.) **397**, 131 (2007).

[20] P. J. Brown and J. C. Matthewman, Institut Laue-Langevin, Report No. CCSLRAL 93-009, 1993 (unpublished).

[21] B. G. Wybourne, *Spectroscopic Properties of Rare Earths* (Wiley, New York, 1965).

[22] K. W. H. Stevens, Proc. Phys. Soc., London, Sect. A **65**, 209 (1952).

[23] M. T. Hutchings, Solid State Physics **16**, 227 (1964).

[24] I. Mirebeau, A. Apetrei, J. Rodríguez-Carvajal, P. Bonville, A. Forget, D. Colson, V. Glazkov, J. P. Sanchez, O. Isnard, and E. Suard, Phys. Rev. Lett. **94**, 246402 (2005).

[25] H. B. Cao, A. Gukasov, I. Mirebeau, P. Bonville, C. Decorse, and G. Dhalenne, Phys. Rev. Lett. **103**, 056402 (2009).

[26] B. Z. Malkin, T. T. A. Lummen, P. H. M. van Loosdrecht, G. Dhalenne, and A. R. Zakirov, J. Phys. Condens. Matter **22**, 276003 (2010).

[27] J. D. Thompson, P. A. McClarty, and M J. P. Gingras, J. Phys. Condens. Matter **23**, 164219 (2011).

[28] A. P. Sazonov, A. Gukasov, H. B. Cao, P. Bonville, E. Ressouche, C. Decorse, and I. Mirebeau, Phys. Rev. B **88**, 184428 (2013).

[29] B. Bleaney, Physica **69**, 317 (1973).

[30] B. Z. Malkin and V. V. Klekovkina (unpublished).

[31] H. Kadowaki, H. Takatsu, T. Taniguchi, B. Fåk, and J. Ollivier, SPIN **5**, 1540003 (2015).